AGU PUBLICATIONS

JGR

Journal of Geophysical Research: Space Physics

RESEARCH ARTICLE
10.1002/2017JA024802

Key Points:
- Ionospheric upflow events with fluxes exceeding 10^{13} m^{-2} s^{-1} analyzed from a large data set of field-aligned profiles
- Ion upflow newly categorized classifies the upflow events into low, medium, and high-flux upflows and investigated for different *Kp* levels
- Seasonal and diurnal occurrence of ion upflow show a distribution peaked around local noon with wider enhancement in the low-flux upflow

Correspondence to:
T. W. David,
david.testimony@yahoo.com

Citation:
David, T. W., Wright, D. M., Milan, S. E., Cowley, S. W. H., Davies, J. A., & McCrea, I. (2018). A study of observations of ionospheric upwelling made by the EISCAT Svalbard Radar during the International Polar Year campaign of 2007. *Journal of Geophysical Research: Space Physics*, *123*, 2192–2203. https://doi.org/10.1002/2017JA024802

Received 20 SEP 2017
Accepted 25 FEB 2018
Accepted article online 1 MAR 2018
Published online 9 MAR 2018

A Study of Observations of Ionospheric Upwelling Made by the EISCAT Svalbard Radar During the International Polar Year Campaign of 2007

T. W. David[1,2], D. M. Wright[1], S. E. Milan[1], S. W. H. Cowley[1], J. A. Davies[3], and I. McCrea[3]

[1]Department of Physics and Astronomy, University of Leicester, Leicester, UK, [2]Department of Physics, Olabisi Onabanjo University, Ago-Iwoye, Nigeria, [3]Rutherford Appleton Laboratory, Didcot, UK

Abstract We have used EISCAT Svalbard Radar data, obtained during the International Polar Year 2007 campaign, to study ionospheric upflow events with fluxes exceeding 10^{13} m^{-2} s^{-1}. In this study, we have classified the upflow events into low, medium, and high flux upflows, and we report on the incidence and seasonal distribution of these different classes. It is observed that high upflow fluxes are comparatively rare and low flux upflow events are a frequent phenomenon. Analysis shows that occurrence peaks around local noon at 31%, 16%, and 2% for low, medium, and high-flux upflow, respectively, during geomagnetically disturbed periods. In agreement with previous studies on vertical and field-aligned flows, ion upflow is observed to take place over a wide range of geomagnetic conditions, with downflow flux occurrence being lower than upflow occurrence. In contrast to previous observations, however, the upflow occurrence is greater around noon during highly disturbed geomagnetic conditions than for moderate geomagnetic conditions. Analysis of the seasonal distribution reveals that, while high-flux upflow has its peak around local noon in the summer, with its occurrence being driven predominantly by high geomagnetic disturbance, the occurrence of low-flux upflow is broadly distributed across all seasons, geomagnetic activity conditions, and times of day. The medium-flux upflow events, although distributed across all seasons, show an occurrence peak strongly related to high *Kp*. Furthermore, during highly disturbed conditions, the low-flux and medium-flux upflow events show a minimum occurrence during the winter, whereas minimum occurrence for the high-flux upflow events occurs in autumn.

1. Introduction

Under the right conditions, heavy ions in the upper atmosphere can outflow into the magnetosphere to influence the dynamics in the coupled solar wind-magnetosphere-ionosphere system. Plasma originating from the ionosphere and entering the magnetosphere forms a substantial part of the plasma that populates the magnetosphere. Strangeway et al. (2005) noted that the Alfvén speed slows down when mass from ionospheric outflows is added to magnetospheric flux tubes. This speed reduction thus affects the way in which the magnetosphere responds to changes in external drivers. The upwelling of these heavy ions is also a process that can, over geological timescales, lead to the loss of planetary atmospheres. Landmark papers (e.g., André & Yau, 1997; Jones et al., 1988; Yau & André, 1997) demonstrate that the main mechanisms responsible for the initial upflow are Joule heating from current closure in the ionosphere and the ambipolar electric field, where the ambipolar potential drop is determined both by suprathermal electrons generated by solar radiation, that is, ionospheric photoelectrons, as well as by electron precipitation (see also the schematic representation from Moore and Khazanov (2010) and Strangeway et al. (2005)).

Dessler and Hanson (1961) were the first to discuss the ionosphere as a source of magnetospheric plasma. They recognized that the terrestrial ionosphere is a large potential source of plasma, especially for light ions at high latitudes outside the plasmasphere. Dessler and Michel (1966) extended this theme, exploring the formation of a steady polar ionosphere outflow into the magnetosphere (see also Moore et al., 1999, and the references therein). Brinton et al. (1971) and Hoffman et al. (1974) established that there is an ionospheric supply of light ion plasma of polar wind origin to the magnetosphere, using observations from ion mass spectrometers on the Explorer 32 and Isis 2 satellites, respectively.

The initial assumption thus was that the only notable ion outflow from the polar cap ionosphere was the light ion polar wind, first discussed theoretically by Axford (1968). It was envisaged to be made up of H^+ and He^+, with energies of a few electron volts (Shelley et al., 1982). In satellite composition measurements reported by

Shelley et al. (1972), it was first observed that heavy ions of atmospheric origin form a significant component of the magnetospheric plasma. These measurements indicated the occurrence of energetic (few keV) O^+ ion fluxes, larger than those of H^+, at the time of geomagnetic storms. Since then, composition measurements from the Geostationary Earth Orbit Satellites 1 and 2, the Spacecraft Charging AT High Altitude spacecraft, and the International Sun-Earth Explorer, in the high-altitude magnetosphere have shown significant availability of O^+ fluxes throughout the magnetosphere, both in the ring current and the plasma sheet (Waite et al., 1985; Yau et al., 1985). It is now well established that the upper atmosphere supplies outflowing ions from the polar ionosphere that might be capable of populating a significant fraction of the plasma in the Earth's magnetosphere, contributing to both the quiet time light ion plasma and the heavy ion plasma characteristic of active times (Chappell et al., 1987, 2000).

It is believed that wave-particle interactions may be responsible for accelerating upwelling ions, once they reach altitudes above 800–1,000 km, yet much remains to be understood about this acceleration process (Hultqvist et al., 1999; Skjæveland et al., 2014). Khazanov et al. (1998) explained that in the polar cap ionosphere, the force of the ambipolar electric field causing oxygen ions (O^+) to outflow is weaker than that due to gravity. Thus, while light ions generally undergo outflow, heavy ions do not, unless further accelerated.

Intensive investigations into ion upwelling and subsequent outflow from the Earth's upper atmosphere have been undertaken in recent years. André and Yau (1997) and Yau et al. (2011) addressed the theories and observations concerning the way the ions are energized. The regions in which plasma from the ionosphere is accelerated out into the magnetosphere are the plasmasphere, the auroral regions, and polar cap field-line regions (Glocer et al., 2009). Yau et al. (1985) have shown that between the altitudes of 1.5 and 4 Earth radii (R_E), the occurrence of the oxygen ion, O^+, is dominant in the summer compared to the winter months. Several studies have suggested that the magnetic force acting upon a toroidal anisotropic ion velocity distribution can result in outflow, the anisotropy resulting from resonant charge exchange that transfers energy via frictional heating to the ion population (Jones et al., 1988; Winser et al., 1988). Howarth and Yau (2008) have shown that the dawn-dusk asymmetry of the interplanetary magnetic field determines the part of the plasma sheet that is populated by the ions. According to Moore et al. (2014), the growth of the ambipolar electric field, as a result of higher electron pressure gradients caused by an increasing electron temperature, will saturate at some point and start to decline, resulting in a substantial reduction of the upflowing flux. In addition to the theoretically based proposition by Lemaire and Schunk (1992) that there is a steady transport of cold ions from the plasmasphere through the plasmaspheric wind during a period including extended low geomagnetic disturbance, Dandouras (2013), using data from the Cluster spacecraft, has inferred the erosion of plasmaspheric ions into the magnetosphere during low and medium activities. In addition, a statistical study of solar cycle 23 by Ogawa et al. (2009) has shown that ion upwelling is a general phenomenon that occurs at all local times (LTs). Foster et al. (1998) examined ion upflow as a function of ionospheric altitude and plasma temperature, while Endo et al. (2000) investigated the geomagnetic activity dependence of upflow and downflow, using the data from the vertically pointing CP7 experiment on the Tromsø EISCAT VHF radar. André and Yau (1997) confirmed the presence of polar wind ions in the topside ionosphere, up to about 10,000 km altitude, in data from the Dynamics Explorer-1 satellite, while Ogawa et al. (2009, and references therein) found, using DE-2 satellite data, that ion upflow occurrence peaked at around 75° and 65° geomagnetic latitude in the dayside and nightside, respectively. Yuan et al. (2008) reported observations by the Defense Meteorological Satellite Program F-15 satellite during a very intense geomagnetic storm, in which fluxes of upflowing ions of order 10^{14} m^{-2} s^{-1} were observed when upward field-aligned ion velocities exceeded 460 m s^{-1}.

The main aim of this study is to investigate the diurnal and seasonal variability of the ion flux at various levels of geomagnetic activity (determined by the *Kp* index), as observed at *E* and *F* region altitudes by the EISCAT Svalbard Radar (ESR), an Incoherent Scatter Radar (ISR) operated by the European Incoherent Scatter Scientific Association (EISCAT, Rishbeth, 1985). In comparison to some previous studies of upflow events conducted using spacecraft data, ground-based radars have the advantage of providing relatively long homogeneous data sets from a fixed location, covering a wide range of altitudes and geomagnetic conditions. We restrict our attention to events with ion fluxes above a threshold of 10^{13} m^{-2} s^{-1} which have the potential to become an outflow (Wahlund et al., 1992; Wahlund & Opgenoorth, 1989). The data

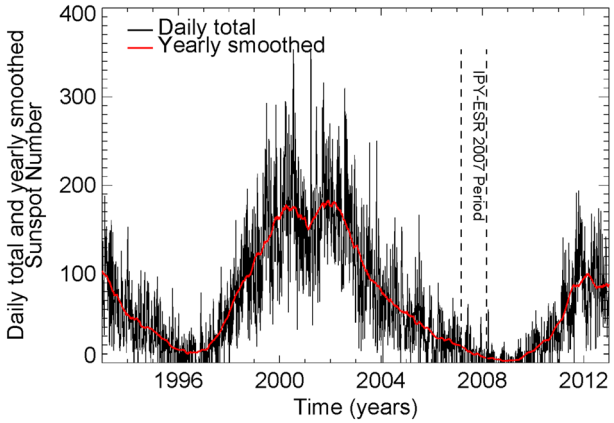

Figure 1. The time series of the daily total (black line) and yearly smoothed (red line) sunspot number.

set comprises the results obtained by the ESR during the third International Polar Year (IPY) campaign. This campaign ran from 2007 to 2009, during which time the ESR 42 m dish was run continuously for about 300 days, measuring 312,444 field-aligned plasma parameter profiles from March 2007 to February 2008, during a period of deep solar minimum. This period is shown in Figure 1, where we plot the time series of the daily total (black line) and yearly smoothed (red line) sunspot numbers. The interval studied here is indicated by the pair of vertical dashed lines. It can be seen that the period of the IPY 2007 campaign corresponds to solar minimum conditions, with yearly smoothed sunspot numbers of 18 for 2007 and 5 for 2008.

Below, the source of data and the filtering technique employed to separate the real signal from noise will be discussed. The analysis of upflow and downflow as a function of *Kp* index will then be presented, followed by an analysis of seasonal occurrence. Finally, we summarize our conclusions.

2. Data Source and Criteria for Data Selection

2.1. Source of Data

The EISCAT Svalbard Radar uses the ISR technique (Williams, 1995) to measure the basic plasma parameters of the ionosphere, including electron density, n_e, from the total scattered energy, ion temperature, T_i, and electron temperature, T_e, from the spectrum shape which is usually double peaked, and the ion drift velocity, v_i, from the ion line Doppler shift. This study uses data obtained from the 42 m diameter fixed dish, measuring the ion drift velocity along the local geomagnetic field line. The data are contained and extracted from the Madrigal online database, which contains a wide variety of ionospheric data from ISRs and other instruments.

The ESR data have a resolution of 1 min and range from about 75 to 500 km in altitude. The average number of data points for each unique time covers the *D*, *E*, and *F* regions with an average ratio of 2:5:9, respectively. An upper limit of 470 km is imposed here on the geodetic altitude, to avoid the low signal-to-noise ratios characterizing much of the high altitude data at solar minimum. A lower altitude limit of 100 km is adopted here. At these low altitudes, the atmosphere is still strongly collisional, making large upflow fluxes unlikely. In addition, the radar data can be susceptible to clutter at close ranges due to the mountainous topography of Svalbard. The ISR measurements are obtained from the ipy_60 pulse code experiment. The range gate size varies along the line-of-sight: increasing from about 3 to 14 km, 15 to 20 km, and 20 to 30 km for altitudes 100–200 km, 201–300 km, and >300 km, respectively. The lateral cross section of the EISCAT beam increases by about 1 km for every 100 km in range, but the increase in illuminated volume with height does not play a significant role in biasing the data, as all densities are calculated per unit volume. The length of the IPY 2007 experiment allowed us to perform a statistical analysis over a long period of ionospheric variations. During the campaign, data were recorded on 81% of the 366 days, with measurements being available for about 70% of the 8,784 hr. The period of November and December 2007 suffered many data gaps due to operational problems (Vlasov et al., 2011).

2.2. Data Filtering

To distinguish between good data and measurements adversely affected by noise, we formulated some additional criteria (supplementary to the data quality flag embedded in the Madrigal database), which were also incorporated into our filtering routine:

1. The flux at the altitude immediately above or below a given point in any profile must not change by a factor greater than 10.
2. The condition in (a) above must also be satisfied for the corresponding altitude in the profiles immediately before and after any given observation.
3. The geodetic altitude of an observation point must be at least 100 km.

Table 1
The Classifications of the Ion Upflow Flux (i.e., Flux Above the Threshold of 10^{13} m^{-2} s^{-1}), Where f_{ion} Indicates Ion Flux

	Ion flux	Class interval	Class frequency
i.	Low	1.0×10^{13} m^{-2} $s^{-1} \leq f_{ion} < 2.5 \times 10^{13}$ m^{-2} s^{-1}	88.3%
ii.	Medium	2.5×10^{13} m^{-2} $s^{-1} \leq f_{ion} < 7.5 \times 10^{13}$ m^{-2} s^{-1}	10.5%
iii.	High	$f_{ion} \geq 7.5 \times 10^{13}$ m^{-2} s^{-1}	1.2%

4. The 0.05% of the data above 470 km has also been expunged because the signal-to-noise ratio drops dramatically; we note that Vlasov et al. (2011) set a cut-off altitude of 450 km when studying traveling ionospheric disturbances using the same data set.

Before applying the above filtering, the data were found to contain several instances of unphysical velocity values in excess of 10 km s^{-1}, whereas previous literature (Blelly et al., 1996; Jones et al., 1988; Wahlund & Opgenoorth, 1989; Winser et al., 1988) shows that the drift velocity of upwelling ions generally remains below a thousand meters per second ($v_i < 1{,}000$ m s^{-1}). The incorporation of the filter described above removed many single noisy data points, such that only 0.2% of the remaining data exceeded this velocity.

In some previous studies of ion upflow, events have been sorted on the basis of ion velocity. In this work, however, we have chosen to sort upflow events on the basis of their ion flux, which, in the steady state, should be a conserved quantity along the flux tube. In terms of potential impact on the magnetosphere, the flux of an outflow event seems to be a more significant metric than its speed. We also note that previous authors have used the flux, rather than the speed, as a way of discriminating between upflow and outflow events.

Following the assumption that quasi-neutrality holds for ionospheric plasma ($n_i \approx n_e$), the ion flux is calculated from the ESR data by using equation (1), and any observation that satisfies the filtering conditions set out above is taken as a valid data point.

$$f_{\text{ion}} = n_e \times v_i \tag{1}$$

Wahlund and Opgenoorth (1989) defined a minimum threshold of 10^{13} m^{-2} s^{-1} for an ion flux having the potential of becoming an outflow, while Skjæveland et al. (2014) referred to the same class of events as "strong upflow flux" with plasma temperatures >2,800 K enhancing the possibility of ion escape. Based on the study by Wahlund and Opgenoorth (1989), which found that potential outflow usually correlates with ion upflow fluxes of magnitude 10^{13} m^{-2} s^{-1} and above, a further filter was applied to remove negative values and fluxes below 10^{13} m^{-2} s^{-1}. Events which exceed this threshold are then classified as having low, medium, or high ion flux as presented in Table 1 and the incidence of each type is shown. Each such event may be characterized by multiple altitudes for which the flux threshold is exceeded along a given field-aligned profile. A total of 1,832,559 data points (representing 22% of the available data) are obtained, after filtering. It is worth noting that, for a large data set such as this, uncertainties in incoherent scatter parameter measurements are expected to be dominated by random noise errors (e.g., Williams et al., 1996). These are dependent on signal-to-noise ratio, and the most significant will be removed by not considering the altitudes above 470 km. In any case, such noise errors are random and hence should not bias the statistical behavior in a large data set. The LT at Longyearbyen, which is 2 hr ahead of UT, is used throughout this study. While it might be argued that MLT is a more applicable parameter, we note that MLT has less meaning at higher latitudes, where the effective MLT is highly dependent on geomagnetic conditions. Where the ESR is known to be on closed field lines, field models indicate that MLT at the ESR is 3 hr ahead of UT and magnetic latitude is 75°N.

3. Results and Discussion

The data presented in Table 1 clearly indicate the high-flux upflow events to be a rare occurrence while the low-flux events are a much more frequent phenomenon. About 88% of the upflow fluxes are between 1.0×10^{13} m^{-2} s^{-1} and 2.5×10^{13} m^{-2} s^{-1}, while the remaining ~12% is shared between the medium and high flux events in the ratio of about 9:1.

Figure 2 shows the plots of ionospheric parameters on 14 June 2007, which is a typical example of an ESR parameter plot during the IPY-ESR campaign. The five panels shown in Figure 2 are electron density,

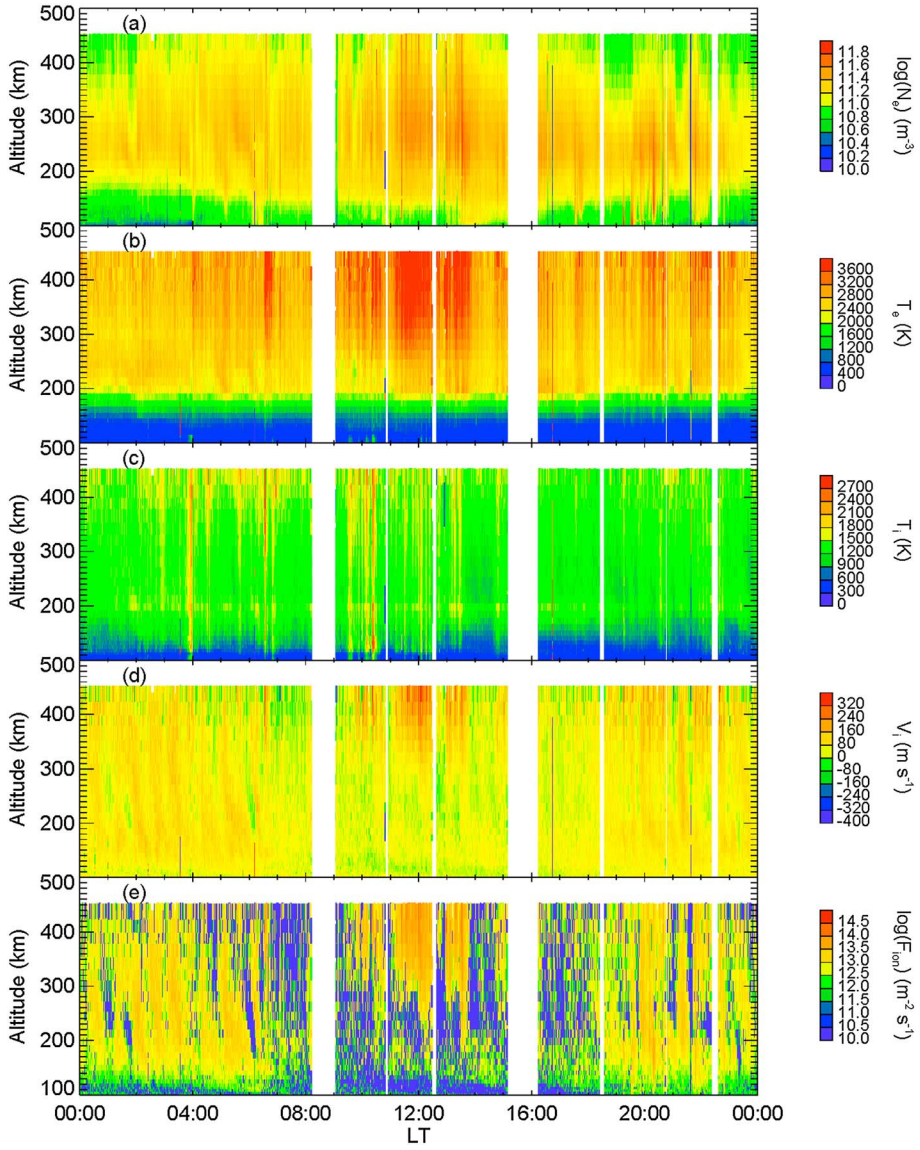

Figure 2. Ionospheric parameters observed by the EISCAT Svalbard Radar (ESR) on 14 June 2007 (a typical example from the 42 m dish during the International Polar Year-ESR campaign) from 22:00 to 00:00 LT on 14 June 2007: (a) electron density, (b) electron temperature, (c) ion temperature, (d) ion drift velocity, and (e) the ion flux.

electron temperature, ion temperature, ion drift velocity, and the ion flux, respectively. The interval begins with moderate nighttime electron density in the *E* region (below 150 km) from 00:00 LT until around 06:00 LT, followed by a short-lived moderately intense precipitation, inferred from the increase in the electron density below 150 km. Additional long duration soft precipitation events, indicated by elevated *F* region electron density, are observed throughout the prenoon and postnoon sectors, while intermittent more intense electron precipitation down to *E* region altitudes occurs in the period from 18 to 24 LT. The second panel shows the enhancements in T_e which occur during the periods of precipitation, especially around local noon, possibly corresponding to cusp conditions, which would favor the creation of an ambipolar electric field, together with an increase in the ion scale height and ion upwelling as a result. Except for few intermittent periods of elevated T_i (shown in the third panel) around 03, 07, and 10 LT, the period is dominated by moderate ion temperature. However, high field-aligned flows corresponding to periods of precipitation are observable around noon and in the premidnight sector, from the velocity plot in Figure 2d. Ion fluxes above the threshold of 10^{13} m^{-2} s^{-1} are observed in the fifth panel, with a maximum flux of 1.8×10^{14} m^{-2} s^{-1} around local noon and 4.7×10^{13} m^{-2} s^{-1} between 20 and 23 LT. OMNI data indicate

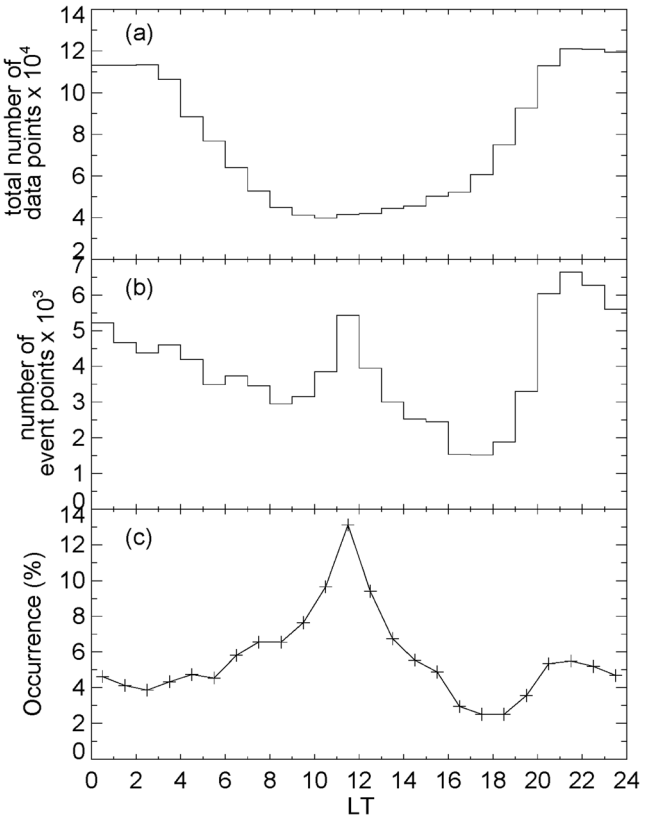

Figure 3. The local time distribution of ion fluxes observed during the International Polar Year-EISCAT Svalbard Radar 2007 campaign: (a) all data points observed by the radar during the period under investigation, (b) event points-data points that satisfy the threshold of 1.0×10^{13} m^{-2} s^{-1}, and (c) percentage of flux that meet the required threshold, that is, (*b*)/(*a*).

that the noon and nightside events are both associated with a southeast orientation of the interplanetary magnetic field clock angle indicating the possibility of geomagnetic reconnection and flux transfer events on the dayside and moderate substorm onset from the analysis of the upper and lower electrojets AU and AL indices (not shown), indicating substorm event on the nightside, respectively.

Figure 3 shows the distribution of upward ion fluxes observed by the EISCAT Svalbard Radar during the entire IPY-ESR 2007 campaign with respect to LT. Figure 3a shows the total number of observations for each hour throughout the campaign, while Figure 3b shows the number of upflow events (above a threshold of 10^{13} m^{-2} s^{-1}) per hour during the same period. Figure 3c shows the percentage ratio of Figure 3b to Figure 3a. The percentage upflow occurrence shows a distinct peak around local noon, which appears consistent with the observational report by Ogawa et al. (2009). However, the occurrence level is lower (by about 25%) compared to their previous work, possibly as a result of the present study coinciding with a deep solar minimum. Outgoing ion flux is, however, observed for 2–13% of the total time, comparable to the estimate of 3–17%, which Ogawa et al. (2009) observed during a complete solar cycle.

3.1. *Kp* Index Analysis of Upflow

Figure 4 shows the temporal distribution of events with low, medium, and high fluxes, as a function of activity level. These are shown as percentages of the time for which such magnetic conditions are encountered. The green, amber, and red colors represent the low, medium, and high values of *Kp* index, respectively. In Figure 4a, where low flux upflow is investigated, the maximum occurrence is below 5% during low geomagnetic conditions ($Kp < 2$), and there is no obvious peak across the LT. However, when *Kp* is either medium or high, a distinct occurrence peak appears around local noon and the enhancement peak is much wider, especially for low flux condition. The highly disturbed periods ($Kp \geq 4$) show a peak of about 31%, while the maximum occurrence encountered during moderate disturbance ($2 \leq Kp < 4$) is ~23%. Another phenomenon observed in this class of low flux events is the dawn and nightside occurrence spikes, which occur during active geomagnetic periods between 5–6 LT and 21–22 LT.

The medium flux events are investigated in Figure 4b, showing that the occurrence frequency increases in magnitude with respect to the level of disturbance as is the case with the low flux. However, the occurrence magnitude for the medium flux events is drastically reduced, with a peak of about 16% and 5% during high and medium *Kp*, respectively, and negligible occurrence during low disturbance. Figure 4c is focused on influence of geomagnetic disturbances on the high flux events and, as for the previous classes, its occurrence peak is observed around local noon, with low values indicating that it is a rare phenomenon. The occurrence peak during high disturbance is about 2%, while at other geomagnetic conditions, the occurrence of high upflow flux is below 0.5%. A small enhancement in all three classes of flux event is observed during high *Kp* between 5 and 6 LT, indicating a possible prenoon asymmetry. However, the peaks observed in the night sector for the low flux upflow events are not evident for the high and medium-flux upflows. The occurrence peaks during high flux and high *Kp* index in the morning, noon, and evening sectors are 0.24%, 2.09%, and 0.03%, respectively, which is equivalent to a percentage ratio of about 10:89:1. Similarly, the analogous ratios for low and medium upflow flux events are 23:56:21 and 15:83:2. This indicates that the high and medium-flux upflow events tend to be highly concentrated around local noon, while the low-flux events are more evenly spread in time. An inference from this is that the low flux events do not exhibit the controlling influence of either the cusp or the auroral oval, while the high and medium flux events seem to be predominantly cusp related.

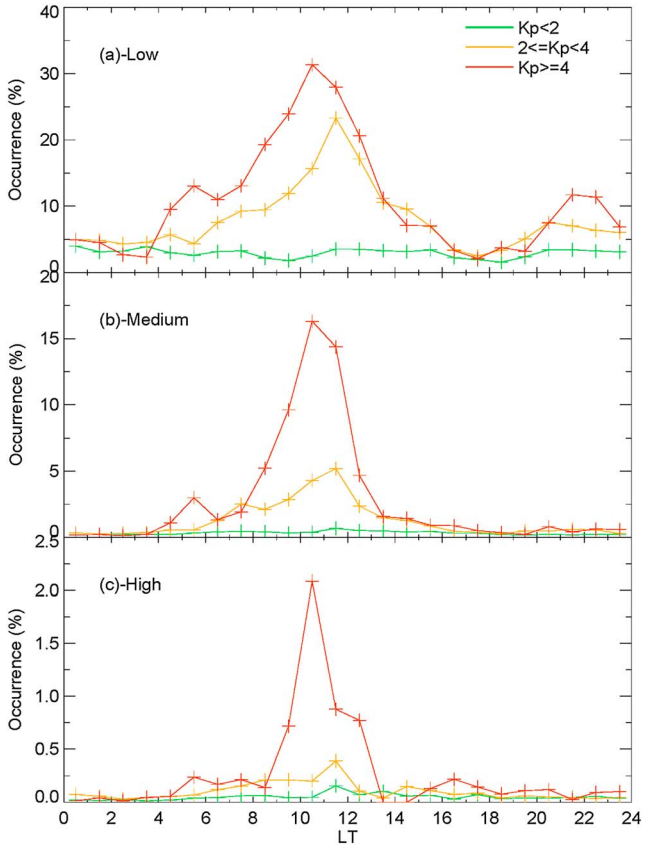

Figure 4. Local time distribution of upflow occurrence in each class in Table 1. This is the percentage ratio of event points to all data points in each local time bin with respect to *Kp* index level and class. The red line indicates $Kp \geq 4$, the amber line indicates $2 \leq Kp < 4$, while the green line shows plots for $Kp < 2$: (a) low, (b) medium, and (c) high flux occurrence.

The occurrence peak for each class of flux is between 10 and 11 LT for the high *Kp* conditions, while it occurs between 11 and 12 LT for moderate disturbance. The peak total occurrence during high geomagnetic disturbance, summing over all three classes of upflow event, is about 50%, which is almost double the peak total occurrence during moderate *Kp*. This is in contrast to the data presented by Ogawa et al. (2009), where the occurrence peak during high disturbance was lower than for medium geomagnetic conditions. These differences in the pattern of ion upflow occurrence in the two studies could be as a result of the Ogawa et al. (2009) study being distributed over a whole solar cycle (700 days from 11 years; 97,000 field-aligned profiles), while the current study uses a near-continuous yearlong data set (300 days from 1 year; 312,444 field-aligned profiles) at solar minimum. Further observation reveals that as expected, the upflow occurrence across all LT is lower in the present study compared to previous studies, characteristic of conditions that, on average, are more active. The only exception is for ion upflow occurrence around the cusp, which is greater by a factor of 2.5 in the present study during high geomagnetic activity ($Kp \geq 4$). A discussion of the upflow flux as a function of the location/magnetic morphology is very interesting and the subject of a forthcoming paper by these authors.

3.2. *Kp* Index Analysis of Downflow

The upwelling ions, unless they are accelerated to gain enough energy to escape, will ultimately experience a downflow due to gravity. In addition, particle precipitation during magnetic reconnection can lead to the injection of particles from either the cusp or the nightside, which can also enhance the downflow flux. We have defined downflow events in this study as those which, in addition to satisfying the filtering conditions in section 2.2, also reach a threshold ion flux of $|f_{ion}| \geq 10^{13}$ m^{-2} s^{-1} arising from a negative (downgoing) velocity. Figure 5 presents the downflow/upflow distribution for the IPY-ESR

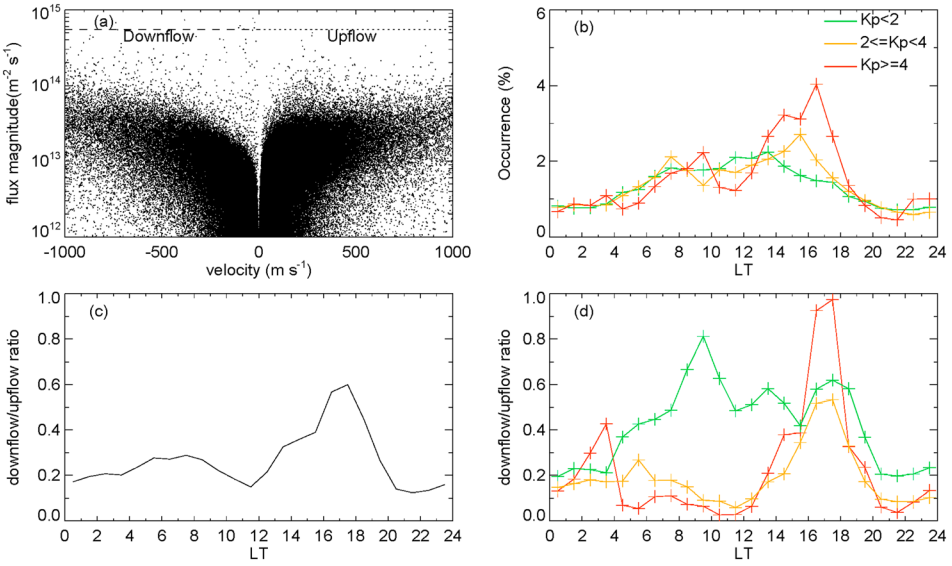

Figure 5. (a) The velocity distribution of ion flux; (b) local time variation of ion downflow occurrence when (i) $Kp < 2$ (green line), (ii) $2 \leq Kp < 4$ (amber line), and (iii) $Kp \geq 4$ (red line); (c) local time variation of total downflow-upflow ratio; (d) hourly variation of ion downflow-upflow ratio when (i) $Kp < 2$ (green line), (ii) $2 \leq Kp < 4$ (amber line), and (iii) $Kp \geq 4$ (red line).

2007 data. Figure 5a shows the velocity distribution of the flux magnitude, where negative and positive values in the horizontal axis refer to the downward and upward motions of the ions indicated by the dashed and dotted lines as marked respectively. While some degree of symmetry is seen in Figure 5a, it is clear that the number of upflow begins to dominate slightly above $|f_{ion}| \geq 10^{13}\,m^{-2}\,s^{-1}$, which agrees with previous studies (Endo et al., 2000; Ogawa et al., 2009) pointing out that upflow events are more commonly observed than downflows at all LT, especially in the cusp and nightside auroral oval (see Figure 5c). Figure 5b presents the occurrence of downflow flux, computed from the ratio of the downflow event points in each LT interval to the total number of data points in the same interval, as a function of *Kp* index. The green, amber, and red colors show the low, medium, and high geomagnetic conditions. Figure 5b suggests that there is little change in downflow occurrence with respect to geomagnetic disturbance level in the prenoon and midnight sectors. However, between 13 and 18 LT, a clear *Kp* dependence is observed, where downflow occurrence increases with increasing disturbance level. The average downflow occurrence in each LT bin is low and does not change much as a function of magnetic activity, being 1.34%, 1.39%, and 1.55%, respectively for low, medium, and high disturbance levels. It is notable that in the period 10–13 LT, there appears to be an inverse relationship between downflow occurrence and *Kp* level. This is precisely the interval in which we already showed that greater magnetic activity tends to increase the number of ion upflow events (see Figure 4). In Figure 5c, the LT distribution of the ratio of the number of downflow to upflow events with $|f_{ion}| \geq 10^{13}\,m^{-2}\,s^{-1}$ is presented. It can be seen that the general trend observed in this 2007 extreme solar minimum data set is for the ratio of downflow to upflow occurrence to have a peak of about 60% (Figure 5c). This agrees with previous studies conducted during periods of higher solar activity (Endo et al., 2000; Ogawa et al., 2009) that showed that the ratio is predominantly less than 1 across all LTs. This result appears to reinforce the conclusion that events with fluxes above this threshold have the potential to become outflow events, which are not necessarily balanced by downflow. The minimum values of downflow/upflow ratio are observed before 04LT, and around local noon and local midnight, which were already identified as periods of increased upflow incidence, as shown in Figure 4a (representing about 88% of the upflow events). Figure 5d shows the downflow/upflow ratio, now separated into different *Kp* levels, where the green, amber, and red colors once again represent the low, medium, and high *Kp* index, respectively. As for ion upflow, it is seen that downflows can occur across the whole range of LTs and geomagnetic conditions. For example, Zhang et al. (2016) noted that even in the polar cap, which is frequently characterized by downflowing plasma, significant ion upflows can be observed in association with polar cap patches. It is clear, however, that the average downflow/upflow ratio for all levels of *Kp* is less than 1 across all LTs, being 42%, 19%, and 22% for low, medium, and high *Kp* conditions, respectively. It is notable that the downflow/upflow ratio is highest at low *Kp* levels across all LTs except for the intervals between 2–4 LT and 16–18 LT where the ratio is higher during periods of high *Kp*. A sharp increase in the downflow/upflow ratio is seen in the 15–18 LT when the geomagnetic disturbance level is high, at which point the upflow and downflow fluxes almost balanced. This is perhaps connected to the injection of plasma on the nightside during substorms, and it is interesting to note that, while the relationship between particle precipitation and ion upflow has received much attention, the potential contribution of precipitation to downflow does not seem to have been so much discussed in the literature. The downflow occurrence in Figure 5b shows similar trends to those reported by Ogawa et al. (2009), indicating that the LT dependence is similar, irrespective of solar activity, but with a smaller peak in this present study at solar minimum.

3.3. Seasonal Analysis of Results

Given its geographic location, there is obviously a very strong seasonal variation in the solar flux and ionization rate above the EISCAT Svalbard Radar. This might intuitively be expected to lead to a seasonal variation in ion upflow events, due to the modulation of electron density. In searching for such a seasonal variation, however, we must take into account the fact that the radar data are often of lower quality during the winter months, due to low signal-to-noise ratio; hence, a smaller fraction of the ESR data satisfies the filtering criteria which we specified earlier.

Figure 6 shows the size of the filtered IPY data set as a function of season and geomagnetic activity level, with Figures 6a to 6d representing spring, summer, autumn, and winter, respectively. The two right-hand panels emphasize the extent to which the winter data set is smaller than that for summer. All panels also show that, in general, the data set contains fewer radar observations in the noon sector than in the midnight sector, across all seasons. While, in general, all seasons contain examples of low, moderate, and high geomagnetic

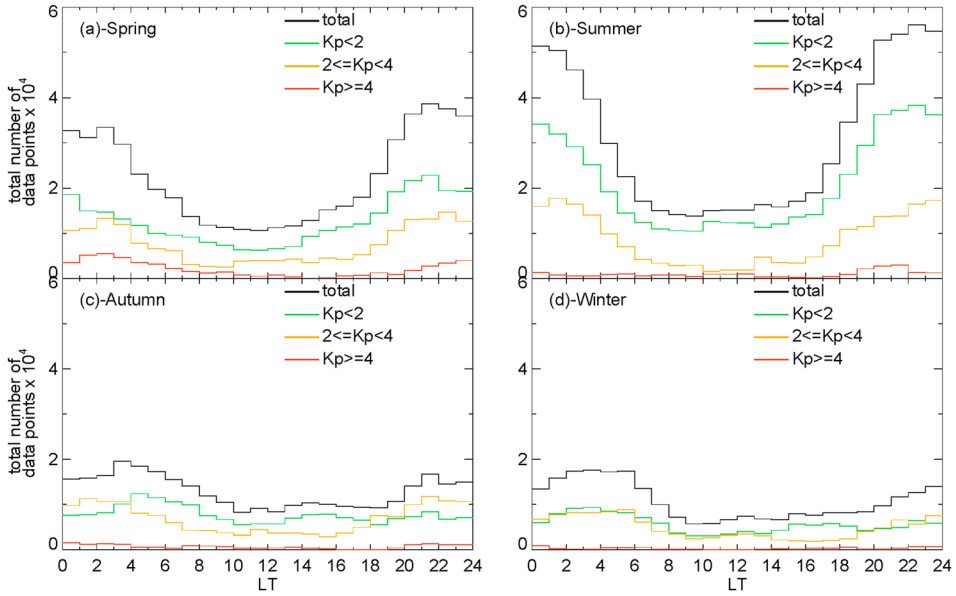

Figure 6. The seasonal local time distribution of total number of flux observed by the radar for all *Kp* data (black line), low *Kp* (green line), medium *Kp* (amber line), and high *Kp* (red line) during (a) spring, (b) summer, (c) autumn, and (d) winter.

activities across all LTs, the winter observations are sufficiently sparse that some LT bins have no examples of high *Kp* conditions ($Kp \geq 4$). Hence, the red traces in the wintertime (lower right) panels are not continuous.

Figures 7–9 show the diurnal variation in percentage occurrence of upflow events for each season, with Figure 7 representing the low-flux events, Figure 8 showing events with moderate flux, and Figure 9 showing the high-flux events. The green, amber, and red traces on each plot represent increasing levels of solar activity, as before.

Not surprisingly, the likelihood of observing low-flux upflow is higher for all seasons of the year. The maximum occurrence of low-flux events during high geomagnetic activity is greater than 30% (Figure 7), while for medium-flux events, the occurrence maximizes in the region 13–22% (Figure 8) and for high flux

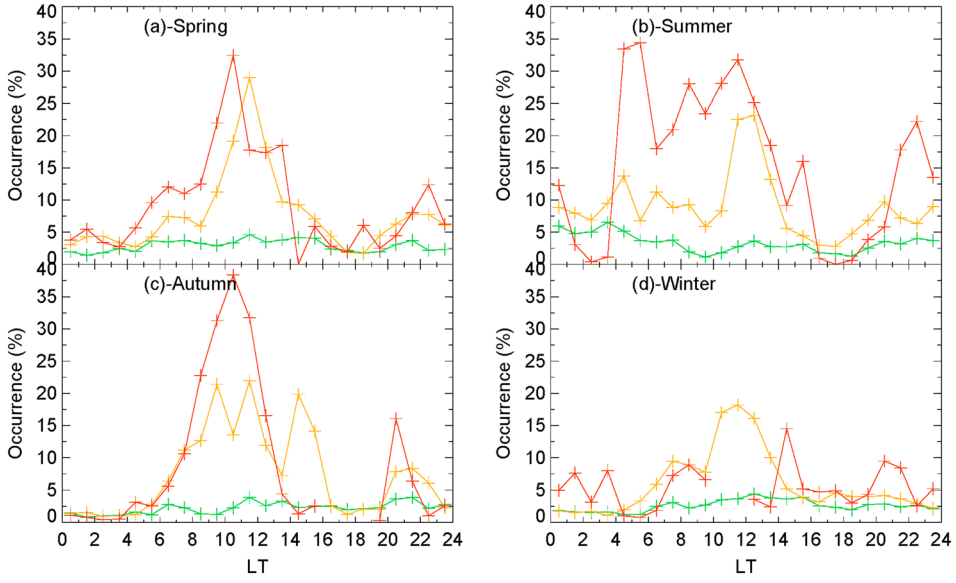

Figure 7. Seasonal occurrence of the low-flux upflow. The red line indicates $Kp \geq 4$, the amber line indicates $2 \leq Kp < 4$, while the green line shows plots for $Kp < 2$. (a) Spring, (b) summer, (c) autumn, and (c) winter.

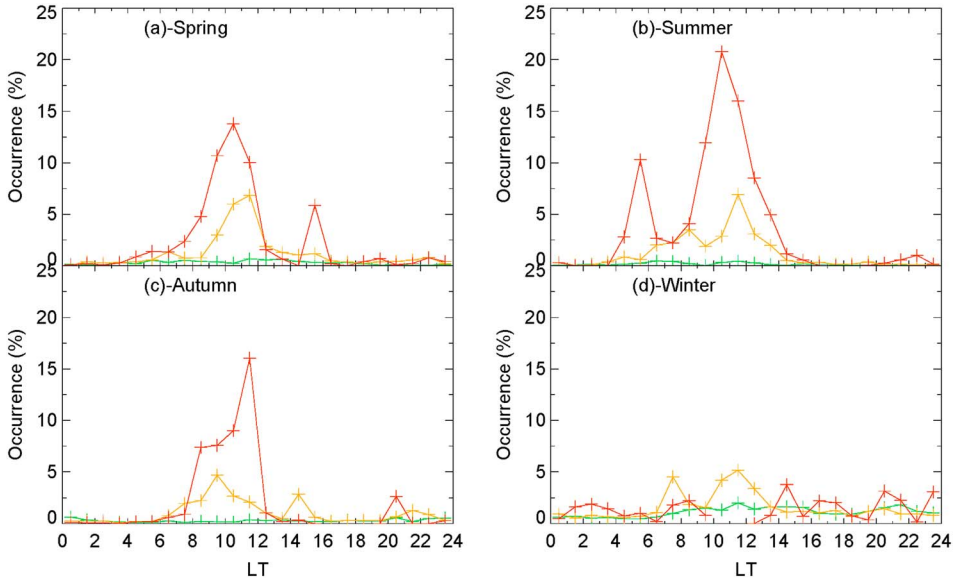

Figure 8. Seasonal occurrence of the medium-flux upflow. The panel and color format are the same as in Figure 7.

in the region 2–5% (Figure 9). This analysis excludes the winter time data, which has too few examples of high activity conditions to enable a meaningful comparison.

For all classes of upflow event, it is notable that no LT dependence is evident under quiet geomagnetic conditions (corresponding to the green traces in Figures 7–9). For higher levels of solar activity (the amber and red traces) the presence of a peak in upflow events around 10–11 LT becomes increasingly noticeable, corresponding to the expected time of the cusp. This peak tends to be broadest in summer and least significant in winter. This may, to some extent, be due to the small size of the winter data set (although the plots have been normalized into percentage occurrence, the statistics are poor for wintertime high *Kp*) but probably also indicates the reduction of ion flux resulting from the absence of solar-produced ionization in winter, when electron densities in the cusp sector are expected to arise primarily from soft particle precipitation.

Outside of the cusp sector, an occurrence peak in the midnight sector is to some extent evident at all seasons for the low-flux events shown in Figure 7, though it is apparently not present for higher fluxes. The size of this

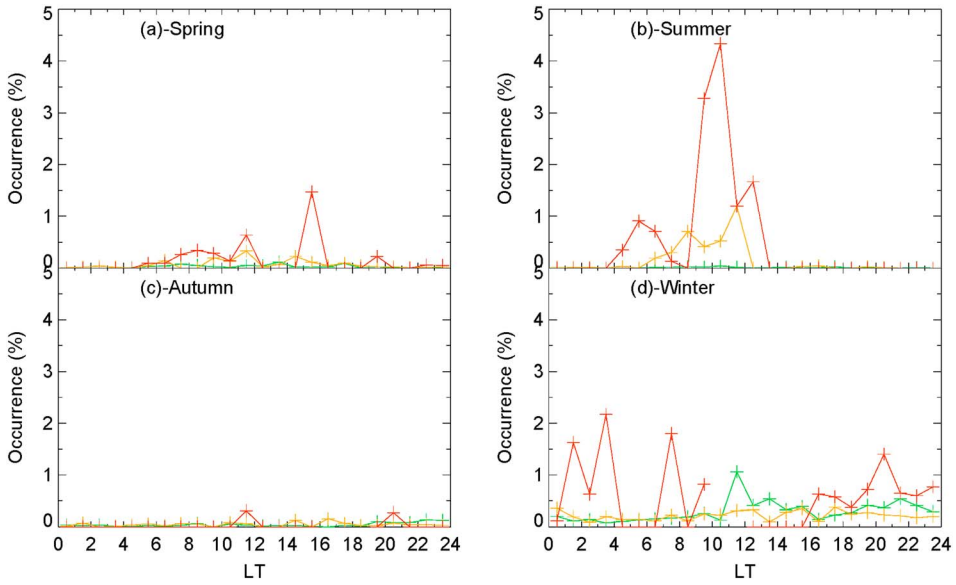

Figure 9. Seasonal occurrence of the high-flux upflow. The panel and color format are the same as in Figure 7.

midnight sector peak increases with increasing *Kp*, suggesting a relationship with the aurora, though the main oval is often well to the south of Svalbard in the midnight sector at these activity levels.

In general, it seems likely that the probability of upflow occurrence increases with geomagnetic activity and that events with higher flux are progressively less prevalent than those with lower flux, irrespective of season.

4. Summary and Conclusions

We have investigated the ionospheric upwelling events observed by the EISCAT Svalbard Radar (ESR) during a yearlong continuous series of deep solar minimum measurements, made as part of the IPY collaboration in 2007. Previous studies in the field chose the ion velocity as the basis for identifying events, but in this work, we have chosen the ion flux because it is a conserved quantity along the flux tube (for approximately constant magnetic field strength). A summary of the main results of this study is as follows:

1. The incidence of upgoing ion flux ($\geq 10^{13}$ m^{-2} s^{-1}) progressively reduces as the level of flux increases, across all seasons and activity conditions. In quantitative terms, events with upward fluxes in the range 1 to 2.5×10^{13} m^{-2} s^{-1} have approximately 10 times higher incidence than events with fluxes above 2.5×10^{13} m^{-2} s^{-1}.
2. Upflow occurrence maximizes around local noon for all classes of upflow, in all likelihood corresponding to the ionospheric projection of the cusp.
3. A lower magnitude of upflow occurrence has been observed during solar minimum, compared to previous studies on over a wider range of solar cycle conditions.
4. In agreement with previous studies, where the ratio of downflow to upflow occurrence was observed to be less than 1 (Endo et al., 2000; Ogawa et al., 2009), downflow occurrence is observed less frequently than upflow at all LTs.
5. Low-flux ion upflows and downflows are common phenomena, which can occur for all levels of geomagnetic activity. This is in good agreement with previous studies from EISCAT VHF radar data at Tromsø (Endo et al., 2000) and ESR data (Ogawa et al., 2009).
6. Occurrence increases for all classes of ion upflow as the level of geomagnetic disturbance increases, whereas there is little or no significant change in occurrence frequency of ion downflow events as the *Kp* level changes. Although the relationship between geomagnetic activity and the downflow/upflow ratio is not linear, a higher ratio of downflow to upflow events is generally observed when *Kp* is low.
7. High-flux upflow is a rare event, with its peak occurring around local noon, whose occurrence frequency depends predominantly on geomagnetic activity. This dependence on geomagnetic activity is visible for all classes of upflow event, though low-flux upflows are much more broadly distributed across all LTs.
8. The cusp sector peak in upflow occurrence is visible in all seasons but is broadest and most pronounced in summer, when ionospheric densities are enhanced by solar production. An additional premidnight occurrence peak is seen in the case of low-flux upflow events and is also clearest in summer. The premidnight peak is not seen in the case of medium or high-flux events.

Acknowledgments
The authors appreciate the efforts of the international community for the 2007 International Polar Year campaign and the EISCAT Scientific Association for making the data observed by the ESR freely accessible on the Madrigal website. This research is sponsored by the Tertiary Education Trust Fund (TETFund) of Nigeria through the Olabisi Onabanjo University, Ago-Iwoye, Nigeria, and Science and Technology Facilities Council (STFC) (ST/N000749/1).

References

André, M., & Yau, A. (1997). Theories and observations of ion energization and outflow in the high latitude magnetosphere. *Space Science Reviews*, *80*(1/2), 27–48. https://doi.org/10.1023/A:1004921619885

Axford, W. I. (1968). The polar wind and the terrestrial helium budget. *Journal of Geophysical Research*, *73*(21), 6855–6859. https://doi.org/10.1029/JA073i021p06855

Blelly, P. L., Robineau, A., & Alcaydé, D. (1996). Numerical modelling of intermittent ion outflow events above EISCAT. *Journal of Atmospheric and Terrestrial Physics*, *58*(1–4), 273–285. https://doi.org/10.1016/0021-9169(95)00035-6

Brinton, H. C., Grebowski, J. M., & Mayr, H. G. (1971). Altitude variation of ion composition in midlatitude trough region—Evidence for upward plasma flow. *Journal of Geophysical Research*, *76*(16), 3738–3745. https://doi.org/10.1029/JA076i016p03738

Chappell, C. R., Giles, B. L., Moore, T. E., Delcourt, D. C., Craven, P. D., & Chandler, M. O. (2000). The adequacy of the ionospheric source in supplying magnetospheric plasma. *Journal of Atmospheric and Solar: Terrestrial Physics*, *62*(6), 421–436. https://doi.org/10.1016/S1364-6826(00)00021-3

Chappell, C. R., Moore, T. E., & Waite, J. H. (1987). The ionosphere as a fully adequate source of plasma for the Earth's magnetosphere. *Journal of Geophysical Research*, *92*(A6), 5896–5910. https://doi.org/10.1029/JA092iA06p05896

Dandouras, I. (2013). Detection of a plasmaspheric wind in the Earth's magnetosphere by the Cluster spacecraft. *Annales Geophysicae*, *31*(7), 1143–1153. https://doi.org/10.5194/angeo-31-1143-2013

Dessler, A. J., & Hanson, W. B. (1961). Possible energy source for the aurora. *Astrophysical Journal*, *134*, 1024–1025. https://doi.org/10.1086/147241

Dessler, A. J., & Michel, F. C. (1966). Plasma in the geomagnetic tail. *Journal of Geophysical Research*, *71*(5), 1421–1426. https://doi.org/10.1029/JZ071i005p01421

Endo, M., Fujii, R., Ogawa, Y., Buchert, S. C., Nozawa, S., Watanabe, S., & Yoshida, N. (2000). Ion upflow and downflow at the topside ionosphere observed by the EISCAT VHF radar. *Annales Geophysicae*, *18*(2), 170–181. https://doi.org/10.1007/s00585-000-0170-3

Foster, C., Lester, M., & Davies, J. A. (1998). A statistical study of diurnal, seasonal and solar cycle variations of F-region and topside auroral upflows observed by EISCAT between 1984 and 1996. *Annales Geophysicae*, *16*(10), 1144–1158. https://doi.org/10.1007/s00585-998-1144-0

Glocer, A., Toth, G., Gombosi, T., & Welling, D. (2009). Modeling ionospheric outflows and their impact on the magnetosphere, initial results. *Journal of Geophysical Research*, *114*, A05216. https://doi.org/10.1029/2009JA014053

Hoffman, J. H., Dodson, W. H., Lippincott, C. R., & Hammack, H. D. (1974). Initial ion composition results from Isis 2 satellite. *Journal of Geophysical Research*, *79*(28), 4246–4251. https://doi.org/10.1029/JA079i028p04246

Howarth, A., & Yau, A. W. (2008). The effects of IMF and convection on thermal ion outflow in magnetosphere-ionosphere coupling. *Journal of Atmospheric and Solar: Terrestrial Physics*, *70*(17), 2132–2143. https://doi.org/10.1016/j.jastp.2008.08.008

Hultqvist, B., Øieroset, M., Paschmann, G., & Treumann, R. (Eds.) (1999). *Magnetospheric plasma sources and losses* (1999th ed.). Dordrecht, Boston, London: Kluwer Academic Publishers. https://doi.org/10.1007/978-94-011-4477-3

Jones, G. O. L., Williams, P. J. S., Winser, K. J., Lockwood, M., & Suvanto, K. (1988). Large plasma velocities along the magnetic-field line in the auroral-zone. *Nature*, *336*(6196), 231–232. https://doi.org/10.1038/336231a0

Khazanov, G. V., Liemohn, M. W., Krivomtsky, E. N., & Moore, T. E. (1998). Generalized kinetic description of a plasma in an arbitrary field-aligned potential energy structure. *Journal of Geophysical Research*, *103*(A4), 6871–6889. https://doi.org/10.1029/97JA03436

Lemaire, J., & Schunk, R. W. (1992). Plasmaspheric wind. *Journal of Atmospheric and Terrestrial Physics*, *54*(3–4), 467–477. https://doi.org/10.1016/0021-9169(92)90026-H

Moore, T. E., Chandler, M. O., Chappell, C. R., Comfort, R. H., Craven, P. D., Delcourt, D. C., et al. (1999). Polar/TIDE results on polar ion outflows. In J. L. Burch, R. L. Carovillano, & S. K. Antiochos (Eds.), *Sun-Earth plasma connections, Geophysical Monograph* (Vol. 109, pp. 87–101). American Geophysical Union.

Moore, T. E., Fok, M.-C., & Garcia-Sage, K. (2014). The ionospheric outflow feedback loop. *Journal of Atmospheric and Solar: Terrestrial Physics*, *115-116*, 59–66. https://doi.org/10.1016/j.jastp.2014.02.002

Moore, T. E., & Khazanov, G. V. (2010). Mechanisms of ionospheric mass escape. *Journal of Geophysical Research*, *115*, A00J13. https://doi.org/10.1029/2009JA014905

Ogawa, Y., Buchert, S. C., Fujii, R., Nozawa, S., & van Eyken, A. P. (2009). Characteristics of ion upflow and downflow observed with the European Incoherent Scatter Svalbard radar. *Journal of Geophysical Research*, *114*, A05305. https://doi.org/10.1029/2008JA013817

Rishbeth, H. (1985). Coherence from incoherence. *Nature*, *313*, 431–432.

Shelley, E. G., Peterson, W. K., Ghielmetti, A. G., & Geiss, J. (1982). The polar ionosphere as a source of energetic magnetospheric plasma. *Geophysical Research Letters*, *9*(9), 941–944. https://doi.org/10.1029/GL009i009p00941

Shelley, E. G., Sharp, R. D., & Johnson, R. G. (1972). Satellite observations of energetic heavy-ions during a geomagnetic storm. *Journal of Geophysical Research*, *77*(31), 6104–6110. https://doi.org/10.1029/JA077i031p06104

Skjæveland, Å., Moen, J., & Carlson, H. C. (2014). Which cusp upflow events can possibly turn into outflows? *Journal of Geophysical Research: Space Physics*, *119*, 6876–6890. https://doi.org/10.1002/2013JA019495

Strangeway, R. J., Ergun, R. E., Su, Y. J., Carlson, C. W., & Elphic, R. C. (2005). Factors controlling ionospheric outflows as observed at intermediate altitudes. *Journal of Geophysical Research*, *110*, A03221. https://doi.org/10.1029/2004JA010829

Vlasov, A., Kauristie, K., van de Kamp, M., Luntama, J. P., & Pogoreltsev, A. (2011). A study of traveling ionospheric disturbances and atmospheric gravity waves using EISCAT Svalbard Radar IPY-data. *Annales Geophysicae*, *29*(11), 2101–2116. https://doi.org/10.5194/angeo-29-2101-2011

Wahlund, J. E., & Opgenoorth, H. J. (1989). Eiscat observations of strong ion outflows from the F-region ionosphere during auroral activity—Preliminary results. *Geophysical Research Letters*, *16*(7), 727–730. https://doi.org/10.1029/GL016i007p00727

Wahlund, J. E., Opgenoorth, H. J., Haggstrom, I., Winser, K. J., & Jones, G. O. L. (1992). EISCAT observations of topside ionospheric ion outflows during auroral activity—Revisited. *Journal of Geophysical Research*, *97*(A3), 3019–3037. https://doi.org/10.1029/91JA02438

Waite, J. H., Nagai, T., Johnson, J. F. E., Chappell, C. R., Burch, J. L., Killeen, T. L., et al. (1985). Escape of suprathermal O^+ ions in the polar-cap. *Journal of Geophysical Research*, *90*(A2), 1619–1630. https://doi.org/10.1029/JA090iA02p01619

Williams, P. J. S. (1995). A multi-antenna capability for the EISCAT Svalbard Radar. *Journal of Geomagnetism and Geoelectricity*, *47*(8), 685–698. https://doi.org/10.5636/jgg.47.685

Williams, P. J. S., Etemadi, A., McCrea, I. W., & Todd, H. (1996). Errors due to random noise in velocity measurement using incoherent scatter radar. *Annales Geophysicae*, *14*(12), 1480–1486. https://doi.org/10.1007/s005850050409

Winser, K. J., Jones, G. O. L., & Williams, P. J. S. (1988). Large field-aligned velocities observed by EISCAT. *Journal of Atmospheric and Terrestrial Physics*, *50*(4–5), 379–382. https://doi.org/10.1016/0021-9169(88)90022-0

Yau, A. W., & André, M. (1997). Sources of ion outflow in the high latitude ionosphere. *Space Science Reviews*, *80*(1–2), 1–25.

Yau, A. W., Peterson, W. K., & Abe, T. (2011). Influences of the ionosphere, thermosphere and magnetosphere on ion outflows. In W. Liu & M. Fujimoto (Eds.), *The dynamic magnetosphere*, *IAGA Special Sopron Book Series* (Vol. 3, pp. 283–314). Netherlands: Springer. https://doi.org/10.1007/978-94-007-0501-2_16

Yau, A. W., Shelley, E. G., Peterson, W. K., & Lenchyshyn, L. (1985). Energetic auroral and polar ion outflow at DE-1 altitudes—Magnitude, composition, magnetic activity dependence, and long-term variations. *Journal of Geophysical Research*, *90*(A9), 8417–8432. https://doi.org/10.1029/JA090iA09p08417

Yuan, Z.-G., Deng, X.-H., & Wang, J.-F. (2008). DMSP/GPS observations of intense ion upflow in the midnight polar ionosphere associated with the SED plume during a super geomagnetic storm. *Geophysical Research Letters*, *35*, L19110. https://doi.org/10.1029/2008GL035462

Zhang, Q. H., Zong, Q. G., Lockwood, M., Heelis, R. A., Hariston, M., Jiang, J., et al. (2016). Earth's ion upflow associated with polar cap patches: Global and in situ observations. *Geophysical Research Letters*, *43*, 1845–1853. https://doi.org/10.1002/2016GL067897